ERUPTION CHARACTERISITICS OF LUNAR LOCALIZED PYROCLASTIC DEPOSITS BASED ON WATER CONTENT, MINERALOGY, REGOLITH PROPERTIES. D. Trang[1], T. Tonkham[1], J. Filiberto[2], S. Li[1], M. Lemelin[3], and C. M. Elder[4], [1]Hawai'i Institute of Geophysics and Planetology, University of Hawai'i at Mānoa, 1680 East-West Rd., Honolulu, HI 96822 (dtrang@higp.hawaii.edu), [2]Astromaterials Research and Exploration Science (ARES) Division, X13, NASA Johnson Space Center, Houston, TX, [3]Département de Géomatique Appliquée, Université de Sherbrooke, Sherbrooke, QC, [4]Jet Propulsion Laboratory, California Institute of Technology, Pasadena, CA.

Introduction: Lunar pyroclastic deposits are low albedo deposits present throughout the lunar surface including both maria and highlands, nearside and farside, and high latitudes and equatorial regions [e.g., 1]. There are two main types of pyroclastic deposits based upon size: localized (<2500 km^2) and regional pyroclastic deposits (>2500 km^2) [1]. In this study, we focus on the smaller localized pyroclastic deposits.

The first and most detailed study of localized pyroclastic deposits are the deposits in Alphonsus crater [2]. This study included examining the radar and volumetric properties of these deposits. They found that vulcanian-like eruptions are most consistent with their observations. They imagined that a dike intrudes into the crust and creates a cooled basaltic cap. With increasing pressure under the basaltic cap, the pressure eventually overwhelms the surrounding rocks and results in explosive decompression.

Later studies examined several pyroclastic deposits across the lunar surface using radar [2–4], digital terrain models (DTMs) [2,4], visible and near-infrared spectrometers [1,4–7], and a radiometer [4] to determine the mineralogy (e.g., olivine, glass, clinopyroxene, orthopyroxene, and plagioclase), deposit thickness and volume, proportion of juvenile material, radar backscatter, surface rock abundance, and regolith density. These various properties were examined against one another to better group localized pyroclastic deposits and understand how they relate to one another [4].

One of the studies divided pyroclastic deposits into three groups based upon the shape of the 1-µm absorption feature. The three Groups could be interpretated as having highlands and pyroclastic material (Group I), mare and pyroclastic material (Group II), and glass and orthopyroxene material (Group III) [5]. Building on that foundation, another study divided the pyroclastic deposits into four groups based upon their surface rock abundance and glass abundance [4], where deposits are classified based upon low surface rock abundance and high glass abundance (Glassy deposits); high rock abundance, high glass abundance (Blocky deposits); moderate rock abundance and low glass abundance (Crystalline deposits); and high rock abundance and low glass abundance (Indistinct Group).

In addition to these studies, we can now look at their water contents using the new Effective Single Particle Absorption Thickness (ESPAT) parameter map [8]. The ESPAT map measures the strength of the 3-µm absorption feature in single scattering albedo space. The strength of this feature and its relationship to water content has been calibrated to returned samples, which allows for water content to be derived from remote spectral data (i.e., Moon Mineralogy Mapper). The goal of this study is to examine how water content in the pyroclastic deposits varies with respect to the geometric, mineralogic, and physical properties of the localized pyroclastic deposits as measured by a previous study [i.e., 4]. A more complete version of this work is found in [9].

Methods: We examined the water content of 34 localized pyroclastic deposits, which were observed with other data sets [i.e., 4], including Apollo, Alphonsus, Birt E, Compton, Frigoris, Gauss, Grimaldi, J. Herschel, Lavoisier, Mersenius, Messala, and Oppenheimer. We measure both the average water content within the deposit as well as the water content of the area surrounding the deposit. We need to measure the surrounding area because water content varies with respect to latitude as well as the regolith containing exogenic water due to solar wind-induced hydration [8, 10, 11]. To make water content more comparable between deposits, we subtract the background from the deposit to obtain the relative water content of the pyroclastic deposit, which we call the excess water abundance. To calculate the water abundance of the deposit or the surrounding area, we average the water content of all the pixels in the deposit or surrounding area.

Results: In obtaining the excess water abundance for each pyroclastic deposit, we found that only five pyroclastic deposits exhibit negative values (i.e., surrounding area had a higher water abundance than the deposit). However, these negative excess water abundances are small (<-10 ppm), with the exception of Apollo, which has an excess water abundance of -73 ppm.

In comparing the excess water abundance to the mineralogy of the deposit, we found strong relationships between excess water abundance and clinopyroxene and glass abundance. In comparing with clinopyroxene (Fig.

1a), we observe an increase in excess water abundance with decreasing clinopyroxene abundance. However, there are at least one deposit that falls off the curve with very low excess water abundance and high clinopyroxene (i.e., Apollo) and five deposits that are low in clinopyroxene with no excess water abundance. All of these deposits are located in Compton, Gauss, and Apollo. We consider these six deposits outliers and note the deposit's location for the other three subfigures (i.e., Figure 1b–d).

In comparing glass abundance with excess water abundance, we see the opposite effect (Fig. 1b). By ignoring the outliers, we see that increasing glass abundance is strongly correlated with increasing excess water abundance.

As for the physical aspects of pyroclastic deposits, we observe a weak inverse relationship between surface rock abundance (i.e., rocks >1 m) and excess water abundance and this trend weakens with the exclusion of the outliers (Fig. 1c). We also examined the relationship between excess water abundance and the density scale height of the deposit (H) [12]. Here, we are using the difference in the density scale height of the deposit relative to the surrounding material (ΔH). To interpret this measurement, positive ΔH implies a deposit containing finer material, more rounded grains, loosely packed regolith, and fewer buried blocks relative to the surrounding regolith [4,12]. In contrast, negative ΔH indicate a more densely packed regolith, larger grains, more angular particles, and/or more buried blocks than the surrounding regolith. In Fig. 1d, we observe that ΔH positively correlates with excess water abundance.

Discussion: The crystallinity of the pyroclasts in a deposit is an indicator of the cooling rate [13,14], where fast cooling rates create greater proportion of glass pyroclasts and slow cooling rates create a greater proportion of crystalline pyroclasts (i.e., clinopyroxene); hence, the reverse trend in Fig. 1a and b. These cooling rates are due to the optical density of the plume, where a dense plume will not allow heat to escape easily, allowing the plume to stay hot and slowly cool, whereas an optically thin plume, heat can easily escape allowing pyroclasts to cool faster [13–15]. Because excess water abundance is correlated with pyroxene and glass, this indicates that the water content is tied to optical density of the plume. The optical density is related to either to the volume flux and/or gas content of the eruption [15]. Because of the strong relationship, it is likely that gas content is controlling the eruption rather than volume flux and that excess water abundance represents interior water content. Further, this could also be used to determine the CO content of the eruption as well [16].

The increasing ΔH with increasing excess water abundance could also provide hints to the eruption. Higher excess water abundance causes the regolith to contain fewer large grain sizes, which could indicate that degree of fragmentation increases with excess water abundance.

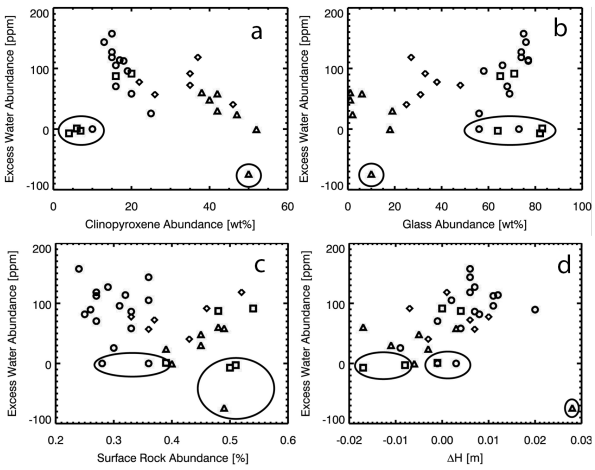

Fig. 1: a) clinopyroxene abundance, b) glass abundance, c) surface rock abundance, and d) ΔH of the localized pyroclastic deposit with respect to excess water abundance of the deposit. Points within the enclosed circle are outliers. Symbols indicate the classification by [4], where circles represent glassy deposits, squares represent blocky deposits, diamonds represent crystalline deposits, and triangles represent indistinct deposits.

References: [1] Gaddis L. R. et al. (2000) *JGR*, 105(E2), 4245–4262. [2] Head, J. W. and Wilson L. (1979) *Proc. Lunar and Planet. Sci. 10th*, 2861–2897. [3] Gaddis, L. R. et al. (1985) *Icarus*, 61, 461–489. [4] Trang, D. et al. (2017) *JGR*, 283, 232–253. [5] Hawke B. R. et al. (1989) *Proc. Lunar and Planet. Sci. 19th*, 255–268. [6] Besse, S. et al. (2014) *JGR*, 119, 355–372. [7] Jawin, E. R. et al. (2015) *JGR*, 120, 1310–1331. [8] Li, S. and Milliken, R. E (2017) *Sci. Adv.*, 3(9), e1701471. [9] Trang, D. et al. (2022) *Icarus*, 375, 114837. [10] McCord, T. B. et al. (2011) *JGR*, 116. [11] Wöhler, C. et al. (2017) *Sci. Adv.*, 3. [12] Hayne, P. O. et al. (2017) *JGR*, 122, 2371–2400. [13] Arndt, J. and von Engelhardt, W. (1987) *Proc. Lunar and Planet. Sci. Conf. 17th*, E372–E376. [14] Arndt, J. et al. (1984), *Proc. Lunar and Planet. Sci. Conf. 15th,* C225–C232. [15] Weitz, C. M. et al (1998) *JGR*, 103, 22725–22759. [16] Wetzel, D. T. et al. (2015) *Nat. Geosci.*, 8, 755–758.